A Letters Journal Exploring the Frontiers of Physics

March 2020

EPL, **129** (2020) 64002 www.epljournal.org
doi: 10.1209/0295-5075/129/64002

Dressed controlled filter with phase transitions of Eu^{3+}: YPO_4 and Pr^{3+}: YPO_4

Habib Ullah[1(a)], Faizan Raza[1], Fahad Nawaz[1], Ali Zamin[1], Jinyang Li[2] and Yanpeng Zhang[1(b)]

[1] *Key Laboratory for Physical Electronics and Devices of the Ministry of Education & Shaanxi Key Lab of Information Photonic Technique, Xi'an Jiaotong University - Xi'an, 710049, China*
[2] *School of Material Science and Engineering, Shaanxi Key Laboratory of Green Preparation and Functionalization for Inorganic Materials, Shaanxi University of Science and Technology - Xi'an, 710021, China*

received 4 November 2019; accepted 8 April 2020
published online 23 April 2020

PACS 42.65.-k – Nonlinear optics
PACS 42.65.Hw – Phase conjugation; photorefractive and Kerr effects

Abstract – We report the spectral and temporal nature of different phases of europium-doped YPO (Eu^{3+}: YPO_4) and praseodymium-doped YPO (Pr^{3+}: YPO_4) crystals. We investigate the change in the dressing effect by shifting the energy levels causing change in line-shape and resolution of the output spectral signal when we employ the hexagonal (H), tetragonal (T), and mixed phase of H and T with different proportions. Further, we propose a tunable spectral filter (narrow bandpass notch filter and bandstop filter) by controlling the dressed phases of Eu^{3+}: YPO_4. The high-resolution dressing peak suggests the realization of the tunable spectral filter with bandwidth contrast of about 93%.

Introduction. – Quantum coherence and quantum excitation have been explored in various rare-earth–doped crystals, suggesting potential and useful advantages of coherent excitation. Recent progress has widely explored solid state atomic coherent materials electromagnetically induced transparency [1], reduction of optical velocity [2], optical storage, which is based on all-optical routing [3], light pulse coherent storage [4] and information that can be stored or erased optically [5]. The crystal structure of YPO_4 exists mainly in two phases, the tetrahedral phase (T-phase) and the hexahedral phase (H-phase) [6,7]. Eu^{3+} (trivalent) ions are very sensitive to site symmetry and host material of the surrounding solid atomic-like media as compared to Ln^{3+} ions [8]. The H-phase YPO_4 crystal doped with Eu^{3+} can be prepared through the hydrothermal method by using trisodium citrate as chelating ligand [9,10]. The Eu^{3+} environment in tetragonal lattice is more symmetric as compared to that in the hexagonal one [11]. The relation between temporal intensity and spectral intensity is changed because of the different crystal structures.

The nonlinear behavior of the crystal can be modified by controlling the transition of bright and dark states via scanning dressing field [12], for the development of quantum communication devices such as tunable hybrid spectral filter. The filter action results from the dressing effect (Autler-Townes (AT) splitting) in spectral or time domain [13]. Moreover, the prediction of a different phase transition with changing gate position of input laser signal could be interesting; such results can find potential applications in optical devices.

In this paper, we discuss the evolution of low-resolution broad peak signal with respect to high-resolution sharp peak signal, observed from different phases of Eu^{3+}: YPO_4 and Pr^{3+}: YPO_4. We report that the dressing effect and resolution of the excited spectrum depend upon the number of contributing energy levels set by the window of gate width. By keeping the gate width narrow (about 100 ns), the intensity output from the number of energy levels can be limited or filtered, while the obtained excitation spectrum results with high resolution and vice versa. We also discuss that the linewidth of the spectral signal changes from broad to sharp by manipulating the gate position, which is exploited for the realization of the tunable spectral filter with optimized bandwidth contrast. The decay process of a strong fluorescence (FL) signal is observed at the zero gate position, while the Stokes signal from spontaneous parametric four-wave mixing (SPFWM)

(a) E-mail: habibdawar987@yahoo.com
(b) E-mail: ypzhang@mail.xjtu.edu.cn (corresponding author)

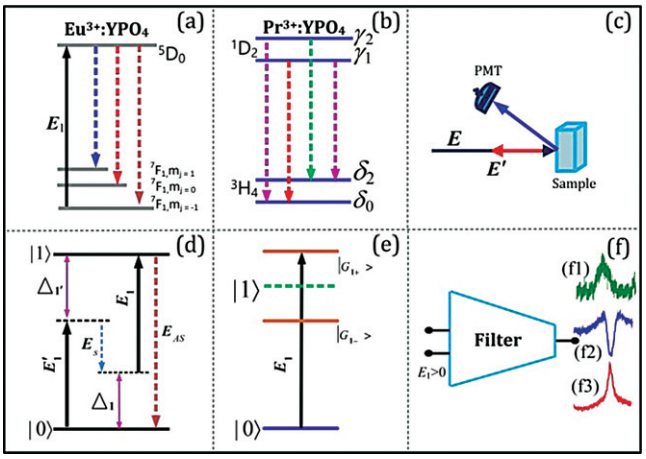

Fig. 1: Fine structure energy levels of (a) Eu^{3+}: YPO_4 and (b) Pr^{3+}: YPO_4. (c) Experimental setup. (d) FWM in two-level system. (e) Dressed energy levels with dark and bright states. (f) Model of tunable spectral filter: (f1) bandpass filter; (f2) narrow bandstop notch filter; and (f3) narrow bandpass notch filter.

decays at a longer gate position. Such a phenomenon suggests a type of filtering of selective wavelengths.

Experimental setup. – Figure 1(a) shows the energy levels of Eu^{3+}: YPO_4. The Eu^{3+}: YPO_4 crystal has triplet ground state $^7F_1$ and singlet excited state $^5D_0$. At low temperature, the triplet state $^7F_1$ splits into $mj = 0$ and $mj = \pm 1$ fine structure levels under the effect of the crystal field. In Pr^{3+}: YPO_4, under the action of the crystal field, the $(2J + 1)$ degeneracy is partly lifted and both $^3H_4$ (ground state) and $^1D_2$ (excited state) levels are split into 2 sub-states each (fig. 1(b)) [14]. Figure 1(c) shows the schematic diagram of the experimental setup. The dye laser (narrow scan with a $0.04\,\mathrm{cm}^{-1}$ linewidth) pumped by an injection-locked single-mode Nd : YAG laser (Continuum Powerlite DLS 9010, 10 Hz repetition rate, 5 ns pulse width) is used to generate the pumping field $\boldsymbol{E}$ (ω, Δ) with frequency detuning $\Delta = \Omega_{mn} - \omega$, where Ω_{mn} is the corresponding atomic transition frequency between levels $|m\rangle$ and $|n\rangle$, ω is the laser frequency. The sample was held in a cryostat maintained at 77 K by flowing through the liquid nitrogen. The pumping field $\boldsymbol{E}$ excites the sample and is reflected ($\boldsymbol{E}'$) from the surface into its original path with a small angle θ. Stokes ($\boldsymbol{E}_\mathrm{S}$) and anti-Stokes ($\boldsymbol{E}_\mathrm{AS}$) signals are generated via SPFWM along with fluorescence (FL), satisfying the phase-matching condition $\boldsymbol{k}+\boldsymbol{k}' = \boldsymbol{k}_\mathrm{S}+\boldsymbol{k}_\mathrm{AS}$ with $\boldsymbol{k}$ being the wave vector. The photomultiplier tube (PMT) is placed to detect the generated composite signals (FL + $\boldsymbol{E}_\mathrm{S}$). The schematic diagram of FWM in a two-level system is illustrated in fig. 1(d) [15]. Figure 1(e) shows dressed energy levels, and fig. 1(f) shows our modeled tunable spectral filter where (f1) represents bandpass filter, (f2) represents narrow bandstop notch filter and (f3) shows narrow bandpass notch filter.

In a two-level system, with a strong pumping field $\boldsymbol{E}$ switched on, the density matrix element of second-order FL generated via perturbation chain $\rho_{00}^{(0)} \overset{E}{\to} \rho_{10}^{(1)} \overset{E'}{\to} \rho_{11}^{(2)}$ can be written as

$$\rho_{11}^{(2)} = \frac{-|G_1|^2}{(\Gamma_{10} + i\Delta_1 + |G_1|^2/\Gamma_{00})(\Gamma_{11} + |G_1|^2/(\Gamma_{10} + i\Delta_1))}, \tag{1}$$

where $G = \mu E/\hbar$ is the Rabi frequency of field $\boldsymbol{E}$ with the electric dipole matrix elements μ_{ij} of levels $|i\rangle$ and $|j\rangle$ and Γ_{ij} is the transverse decay rate. The lifetime of FL is $\Gamma_\mathrm{FL} = \Gamma_{10}+\Gamma_{11}$. The third-order nonlinear density matrix elements of $\boldsymbol{E}_\mathrm{S}$ signal detected at PMT via perturbation chain $\rho_{00}^{(0)} \overset{E_1}{\to} \rho_{10}^{(1)} \overset{E_\mathrm{AS}}{\to} \rho_{00}^{(2)} \overset{E_1'}{\to} \rho_{10(\mathrm{S})}^{(3)}$ is given as

$$\rho_{20(\mathrm{S})}^{(3)} = \frac{-iG_\mathrm{AS}\mathrm{G}_1\mathrm{G}_1'}{(\Gamma_{20}+i\Delta_1)(\Gamma_{00}+i\Delta_1+|\mathrm{G}_1|^2/\Gamma_{00})(\Gamma_{20}+i(\Delta_1+\Delta_1'))}. \tag{2}$$

The lifetime of $\boldsymbol{E}_\mathrm{S}$ is $\Gamma_\mathrm{S} = \Gamma_{00} + \Gamma_{10} + \Gamma_{11}$. The coupling field interaction, the homogeneous linewidth broadening measured for fourth-order fluorescence, is given as $\Gamma_{i/j} = \Gamma_\mathrm{pop} + \Gamma_\mathrm{ion\text{-}spin} + \Gamma_\mathrm{ion\text{-}ion} + \Gamma_\mathrm{phonon} - \Gamma_\mathrm{dressing}$. Since the generation of FL and $\boldsymbol{E}_\mathrm{S}$ emission is simultaneous along with the detection at PMT, one can consider this signal as a composite signal $(\rho_{11}^{(2)} + \rho_\mathrm{S}^{(3)})$.

Results and discussions. – Figures 2(a) and (b) show the spectral intensity of the composite signal (FL + $\boldsymbol{E}_\mathrm{S}$) obtained from mixed phase (much H-phase + less T-phase) of the Eu^{3+}: YPO_4 crystal by scanning $\boldsymbol{E}$ from 580 nm to 605 nm at low power (1 mW) by fixing the gate width at 1 μs and 100 ns, respectively. Second-order FL and third-order Stokes for mixed phase (much H-phase + less T-phase) of Eu^{3+}: YPO_4 can be written as $\rho_{11(H+T)}^{(2)}$ (similar to eq. (1)) and $\rho_{20(\mathrm{S})(H+T)}^{(3)}$ (similar to eq. (2)), respectively, where (H + T) (in $\rho_{11(H+T)}^{(2)}$ and $\rho_{20(\mathrm{S})(H+T)}^{(3)}$) represent density matrix elements of mixed-phase (much H-phase + less T-phase) of Eu^{3+}: YPO_4 for FL and Stokes. Total intensity of composite signal for the mixed phase (much H-phase and less T-phase) is written as $\rho_{(H+T)} = \rho_{11(H+T)}^{(2)} + \rho_{20(\mathrm{S})(H+T)}^{(3)}$. In fig. 2 the excitation spectrum is measured by changing gate positions from 200 ns to 25 μs. Changing the gate width (figs. 2(a), (b)) corresponds to change in the number of energy levels, which affects resolution of spectral signal (from low to high). In fig. 2(b), when the gate width is fixed at 100 ns and the gate position is changed from 200 ns to 25 μs, the observed spectral signal changes gradually from broad peak $\rho_{11(H+T)}^{(2)}$ (fig. 2(b1)) to sharp peak $\rho_{20(\mathrm{S})(H+T)}^{(3)}$ (fig. 2(b4)). Here the competition between $\rho_{11(H+T)}^{(2)}$ and $\rho_{20(\mathrm{S})(H+T)}^{(3)}$ in a composite signal determines the lineshape of the spectral signal which is associated with the lifetime $\Gamma_{(H+T)}$ of its constituents (Γ_FL and Γ_S). Change in the gate position opens a window

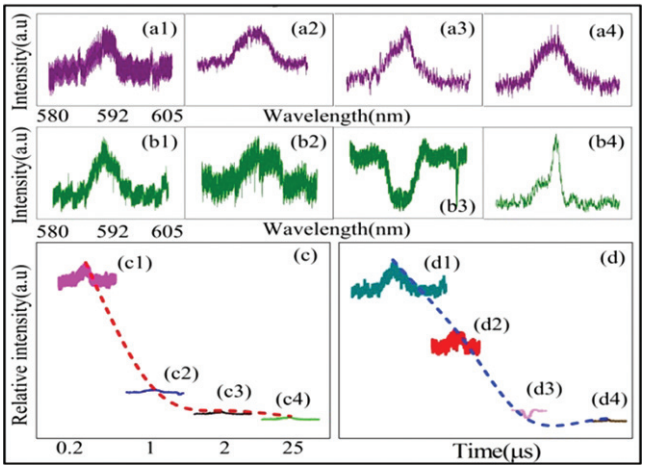

Fig. 2: (a), (b): the spectral intensity from mixed phase (much hexagonal and less tetragonal phase) of Eu^{3+}: YPO_4 crystal measured at different gate positions (200 ns, 1 μs, 2 μs, and 25 μs) when gate width is set at 1 μs and 100 ns, respectively by fixing power at 1 mW. (c), (d): the relative intensity of spectral signal corresponding to the gate position of curves presented in (a) and (b), respectively.

for multi-energy level (like bright to dark states demonstrated in fig. 1(e)) which affects Γ. This can be further explained from the evolution of $\boldsymbol{E}_{\rm S}$ from FL in the composite signal regime. As the lifetime $\Gamma_{{\rm FL}(H+T)}$ of FL is short, ${\rm FL}_{(H+T)}$ dominates at near gate position (200 ns) and the intensity of the composite signal can be modified as $\rho_{(H+T)} = \rho^{(2)}_{11(H+T)}$. Hence, the linewidth ${\rm FL}_{(H+T)}$ of the spectral signal is broad as shown in fig. 2(b1). Further, by increasing gate position from 600 ns to 25 μs, FL emisssion switches to Stokes due to long lifetime of Stokes and composite signal behaves as pure Stokes signal such that $\rho_{(H+T)} = \rho^{(3)}_{20({\rm S})(H+T)}$. Hence, the linewidth of the spectral signal at 25 μs becomes narrow (fig. 2(b4)). At gate position 2 μs (fig. 2(b3)), the ${\rm FL}_{(H+T)}$ peak changes to dressing suppression dip modeled by $|G_1|^2/(\Gamma_{10} + i\Delta_1)$ term (similar to eq. (1)) as the emission is switched from bright state $|G_{1+}\rangle$ to dark state $|1\rangle$ (fig. 1(e)).

When the gate width is set at 100 ns, the resolution of the spectral signal changes from low (broad peak) to high (sharp peak). The spectral intensity signal measured by changing gate position (when the gate width = 100 ns) is shown in fig. 2(b). When the gate width is narrow (100 ns), the observed spectral signal results from a single energy level having single lifetime experiences strong dressing effect resulting in the high resolution of the measured excitation spectrum. When the gate width is increased to 1 μs, no change in the linewidth of the spectral signal is observed with respect to increase in gate position shown in figs. 2(a1)–(a4). Besides, no suppression dip is observed for a broad gate width. This can be explained from broad gate width, which incorporates the contribution of more energy levels (more lifetime and more scattering). It should be noted that more lifetime and more scattering nullify the dressing effect and enhances inter-energy level scattering, resulting in a spectrum with low-resolution broad peak. Figures 2(c) and (d) show relative spectral intensity plotted against different gate positions related to figs. 2(a) and (b), respectively, where the dashed line represents the temporal intensity profile similar to time-domain signal shown in figs. 2(c) and (d).

The tunable spectral filter is realized from the spectral signals observed in fig. 2. Based on our results, two types of spectral filters are realized: one is the narrow bandpass notch filter (NBPNF) and the other is the narrow bandstop notch filter (NBSNF) as illustrated in figs. 1(f3) and (f2), respectively. From our experiment, the bandwidth contrast ($B = \lambda_{c1} - \lambda_{c2}/\lambda_{c1} + \lambda_{c2}$) can be described as a ratio of pass and stop frequencies, where λ_{c1} and λ_{c2} are cutoff wavelengths of spectral signal. When the gate width is 100 ns and the gate position is fixed at 200 ns, the resolution of spectral signal is low, where the cutoff wavelength $\lambda_{\rm c1}$ is 18.9 nm and $\lambda_{\rm c2}$ is 6 nm, so the bandwidth contrast is measured about 51% (fig. 2(b1)) and filter work here as a bandpass filter (fig. 1(f1)). When the gate position increases to 25 μs the resolution of spectral signal becomes high causing bandwidth contrast to increase upto 93% and the filter is switched from bandpass filter to NBPNF (sharp peak) as shown in fig. 1(f3). Furthermore, when the gate position is fixed at 2 μs, the filter is switched to band stop filter (fig. 2(b3)) due to dressing effect (suppression dip) as illustrated in fig. 1(f2), whose bandwidth contrast is 62%. This suggests our proposed filter modeled in fig. 1(f) works as both NBPNF (fig. 1(f3)) and NBSNF (fig. 1(f2)). Based on these characteristics, we characterize such filter as a tunable spectral filter. Moreover, when the gate width is fixed to 1 μs resolution of spectral signal is low (figs. 2(a1)–(a4)) with less bandwidth contrast. At narrow gate width 100 ns, the resolution of the spectral signal is high in fig. 2(b4) and the bandwidth contrast observed is more. This suggests that the bandwidth contrast increases when the gate position increases while gate width is fixed at 100 ns which means a narrow gate width is more useful than broad gate width for our modeled filter. Furthermore, filter gain can be defined as $G = I_b/I_p$ (I_p is the intensity of the pass filter and I_b is intensity stop filter). Maximum filter gain ($G = 2.3$) is observed at 77 K and at a fixed gate position of 20 μs (fig. 2(b3)) with bandwidth contrast of 62%. When the gate position is changed from 2 μs to 25 μs, the filter gain is reduced to 1.5 (fig. 2(a4)).

In subsequent results (figs. 3–6) of Eu^{3+}: YPO_4, spectral intensity of the composite signal is obtained by scanning $\boldsymbol{E}$ when the gate width is fixed at 100 ns and by changing gate positions (200 ns, 1 μs, 2 μs, 5 μs, and 20 μs).

In fig. 3 by increasing the power of $\boldsymbol{E}$ from 1 mW to 2 mW, spectral peak of ${\rm FL}_{(H+T)}$ changes to strong dressing suppression dip (fig. 3(a3)). This can be explained by the switch in the emission from bright state $|G_{1+}\rangle$ to dark state $|1\rangle$ of dressed energy levels shown in fig. 1(e).

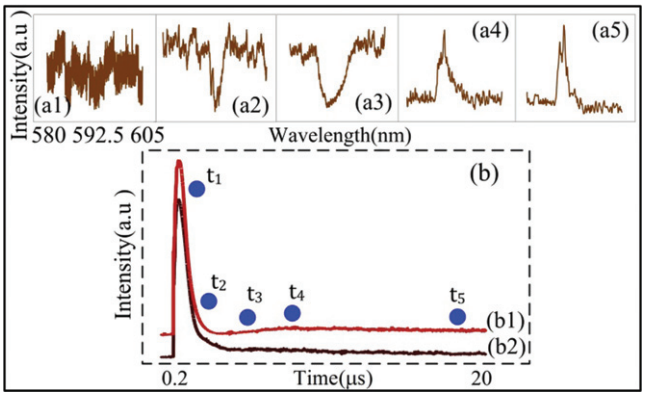

Fig. 3: (a) The spectral intensity signal of mixed phase (much H-phase and less T-phase) of Eu^{3+}: YPO_4 measured at different gate positions when E is scanned from 580 to 605 nm at fixed power of 2 mW and gate width at 100 ns. (b1), (b2): the composite signal measured at resonant and off-resonant wavelength of $\boldsymbol{E}$, respectively.

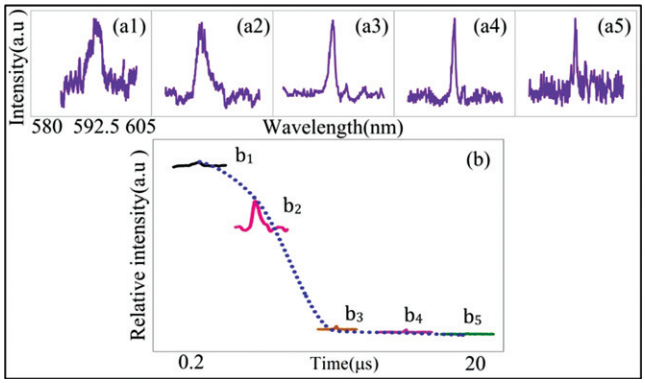

Fig. 4: (a) Spectral intensity signal of pure T-phase Eu^{3+}: YPO_4 measured at different gate positions by fixing power at 1 mW. (b) Relative intensity of the spectral signal corresponding to curves shown in (a).

In fig. 3, when the gate position is increased, the linewidth of the spectral signal changes from broad ($\rho^{(2)}_{11(H+T)}$) to sharp ($\rho^{(3)}_{20(S)(H+T)}$), as explained in detail in fig. 2(b). However, in fig. 3, the linewidth of the spectral signal is sharp with high resolution as compared to fig. 2(b). Figures 3(b1) and (b2) show the composite signal intensity when $\boldsymbol{E}$ is fixed at resonant (588.6 nm) and off-resonant (592 nm) wavelength, respectively. The dressing effect of beam $\boldsymbol{E}$ makes the intensity curves in the time domain at $\Delta_1 = 0$ show Aulter-Townes splitting (AT splitting). One can observe that at the resonant wavelength the splitting is stronger as compared to the off-resonant wavelength. When the gate position changes from 200 ns (fig. 3(a1)) to 1 μs (fig. 3(a2)) and 2 μs (fig. 3(a3)) the bandwidth contrast of filter changes from 60% to 67% and 57%, respectively, and the filter is switched from bandpass filter (fig. 1(f1)) to NBSNF (fig. 1(f2)). By further increasing of gate position to 25 μs the bandwidth contrast is observed to be 71% (fig. 3(a5)) while filter switches from NBSNF (fig. 1(f2)) to NBPNF (fig. 1(f3)).

Figure 4 shows the spectral intensity signal of T-phase Eu^{3+}: YPO_4 measured at different gate positions at low power (1 mW). For T-phase of Eu^{3+}: YPO_4, FL and Stokes can be written as $\rho^{(2)}_{11(T)}$ (similar to eq. (1)) and $\rho^{(3)}_{20(S)(T)}$ (similar to eq. (2)), respectively, where T (in $\rho^{(2)}_{11(T)}$ and $\rho^{(3)}_{20(S)(T)}$) represents density matrix elements of the T-phase of Eu^{3+}: YPO_4 for FL and Stokes. The total intensity of the composite signal for T-phase is $\rho_{(T)} = \rho^{(2)}_{11(T)} + \rho^{(3)}_{20(S)(T)}$. At gate position of 200 ns, the $FL_{(T)}$ emission dominates in the composite signal and intensity of composite signal can be written as $\rho_{(T)} = \rho^{(2)}_{11(T)}$. Here, the spectral signal observed is broad with low resolution (fig. 4(a1)). By increasing the gate position, FL emission starts to decay, Stokes emission dominates FL in a composite signal due to low power. As gate position is increased to 25 μs, $\boldsymbol{E}_{S(T)}$ evolves from $FL_{(T)}$ in the composite signal regime and the intensity of composite signal can be modified as $\rho_{(T)} = \rho^{(3)}_{20(S)(T)}$, where the spectral peak with low linewidth and high resolution is observed in fig. 4(a5). By comparing fig. 3 and fig. 4, the dressing effect in the pure T-phase is weak as no suppression dip is observed. This phenomenon can be explained by pure T-phase Eu^{3+}: YPO_4, due to its strong excitation signal caused by transfer probability. Due to transfer probability, a strong dipole moment appears with symmetry due to D_{2d} group symmetry. However, T-phase behaves less as an atomic-like structure. Figure 4(b) follows similar relative spectral intensity profile discussed in figs. 2(c) and (d). By increasing the gate position from 200 ns to 25 μs the bandwidth contrast changes from 60% (fig. 4(a1)) to 87% (fig. 4(a5)) and the filter is switched from bandpass to NBPNF as shown in figs. 1(f1) and (f3), respectively.

In fig. 5, the total intensity of composite signal for mixed phase (much T-phase + less H-phase) of Eu^{3+}: YPO_4 is $\rho_{(T+H)} = \rho^{(2)}_{11(T+H)} + \rho^{(3)}_{20(S)(T+H)}$, where (T+H) represents the mixed phase (much T-phase + less H-phase) of Eu^{3+}: YPO_4. Similar to figs. 3–5, low-resolution broad FL peak $\rho^{(2)}_{11(T+H)}$ (similar to eq. (1)) changes to high-resolution, sharp $\boldsymbol{E}_S$ peak $\rho^{(3)}_{10(S)(T+H)}$ (similar to eq. (2)) as gate position is increased from 200 ns to 20 μs. As compared to T-phase Eu^{3+}: YPO_4 (fig. 4), the dressing effect in mixed phase (much T-phase + less H-phase) of Eu^{3+}: YPO_4 is stronger as suggested by suppression dip in figs. 5(a2)–(a3). The dressing effect observed in fig. 5 is weaker than the dressing effect of the mixed phase (much H-phase and less T-phase) of Eu^{3+}: YPO_4 (fig. 3) which can be explained from the lower contribution of H-phase than T-phase. The H-phase is more asymmetric (more atomic like) due to D_2 group symmetry, which results in high resolution and sharp spectral signal, whereas the T-phase is more symmetric (less atomic like) resulting in broad

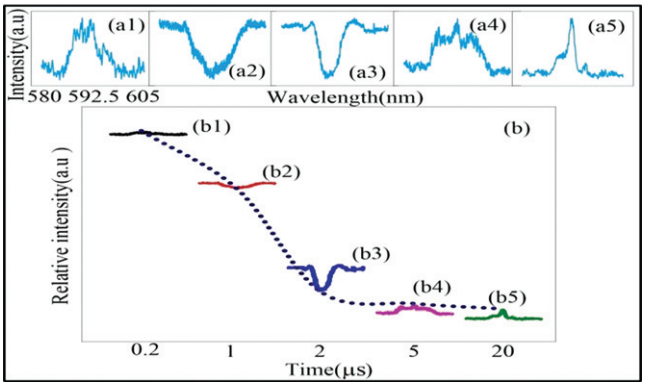

Fig. 5: Spectral intensity signal of mixed phase (much T-phase + less H-phase) of Eu^{3+}: YPO_4 measured at different gate positions by fixing power at 2 mW. (b) Relative intensity of spectral signal corresponding to curves presented in (a).

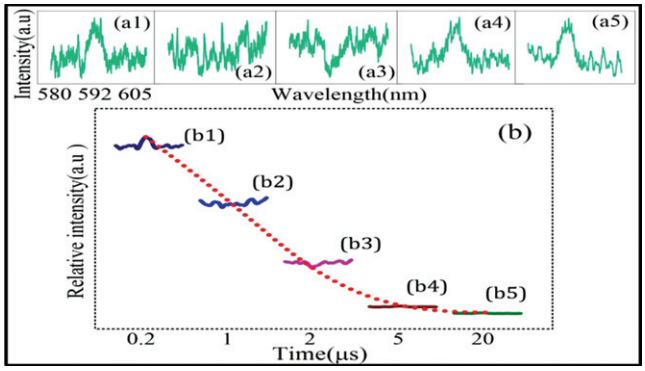

Fig. 6: Spectral intensity signal of pure H-phase Eu^{3+}: YPO_4 measured at different gate positions by fixing power at 2.5 mW. (b) Relative intensity of spectral signal corresponding to curves shown in (a).

signal and low resolution but having strong excitation signal. Figure 5(b) follows similar relative spectral intensity profile discussed in figs. 2(c) and (d). Here the bandwidth contrast changes from 47% (fig. 5(a1)) fig. 1(f1) to 79% (fig. 5(a5)) fig. 1(f3) by changing gate position from 200 ns to 25 μs and the filter switches from bandpass filter (fig. 1(f1)) to NBPNF as shown in fig. 1(f3). Furthermore, when the gate position is fixed at 1 μs and 2 μs in figs. 5(a2) and (a3) the filter switches from bandpass filter fig. 1(f1) to NBSNF fig. 1(f2).

Figure 6 shows the spectral intensity signal of H-phase Eu^{3+}: YPO_4. Here, the total intensity of the composite signal is $\rho_{(H)} = \rho^{(2)}_{11(H)} + \rho^{(3)}_{20(S)(H)}$, where (H) represents H-phase of Eu^{3+}: YPO_4. From fig. 6, one can observe that the lineshape of the spectral signal does not change with the increase in gate position. At gate position 200 ns, FL emission $\rho^{(2)}_{11(H)}$ dominates Stokes $\rho^{(3)}_{20(S)(H)}$ in composite signal and the broad peak is observed in fig. 6(a1). By increasing the gate position at 20 μs fig. 6(a5), the intensity of the composite signal decreases, while the proportion of Stokes $\rho^{(3)}_{20(S)(H)}$ slightly increases but FL still dominates. This can be explained as the FL emission becomes strong when the power is increased to 2.5 mW. Furthermore, when the gate position is fixed at 2 μs, the spectral peak $FL_{(H)}$ changes to weak dressing suppression dip (fig. 6(a3). However, the dressing effect in the H-phase is stronger than in the T-phase (fig. 4) as explained in fig. 5. Figure 6(b) follows similar relative spectral intensity profile as discussed in figs. 2(c) and (d). The bandpass filter switched to NBSNF by increasing the gate position from 200 ns (fig. 6(a1) to 2 μs (fig. 6(a3) with bandwidth contrast 54% and 58%, respectively. By further increasing the gate position to 20 μs (fig. 6(a5) the filter changes from NBSNF to NBPNF with bandwidth contrast 60% as shown in fig. 1(f).

Figure 7 shows the spectral intensity signal obtained from the H-phase (fig. 7(a1)), T-phase (fig. 7(b)) and mixed phase (much H-phase and less T-phase) (fig. 7(c)) of the Pr^{3+}: YPO_4 crystal. The total intensity of H-phase, T-phase and mixed phase (much H-phase and less T-phase) of Pr^{3+}: YPO_4 is modelled as $\rho_{(H)} = \rho^{(2)}_{11(H)} + \rho^{(3)}_{20(S)(H)}$, $\rho_{(T)} = \rho^{(2)}_{11(T)} + \rho^{(3)}_{20(S)(T)}$ and $\rho_{(H+T)} = \rho^{(2)}_{11(H+T)} + \rho^{(3)}_{20(S)(H+T)}$. Since we know that by increasing the gate position, Stokes evolves from FL in a composite signal where the linewidth of the spectral signal becomes sharp, as suggested by the lineshape trend in fig. 2 of Eu^{3+}: YPO_4. In the crystal field of Pr^{3+}: YPO_4, $2J+1$ degeneracy of the levels is partly split and $J = 0, 1, 2, 3, 4, 5, 6$ levels split into 1, 2, 4, 5, 7, 8, 10, respectively. Under this symmetry, two transition levels are allowed: $^1D_2$ (ground state) and $^3H_4$ (excited state) [16]. H-phase YPO crystals are more atomic like and their behavior should have a strong dressing effect; however, no dressed suppression dip is observed in fig. 7(a) and also limited by the weak excitation signal. In figs. 7(b3) and (b4), at gate position of 2 μs and 5 μs dressing suppression dip in spectral signal is observed in the T-phase, as emission is switched from bright state to dark state (fig. 1(e)). A dressing suppression dip is also observed in mixed phase (much H-phase + less T-phase) of Pr^{3+}: YPO_4 at gate position 1 μs (fig. 7(c2)), 2 μs (fig. 7(c3)) and 5 μs (fig. 7(c4)). Hence the dressing effect in the mixed phase (much H-phase+less T-phase) of Pr^{3+}: YPO_4 (fig. 7(c2)) is stronger than in both H-phase (fig. 7(a2)) and T-phase (fig. 7(b2)). Moreover, when the gate position is set at 25 μs, two, three and four sharp spectral peaks are observed in figs. 7(a5), (b5) and (c5), respectively, likely because of different site symmetries.

Comparison of Pr^{3+} (fig. 7(c4)) and Eu^{3+} (fig. 3(a4)) at the power of 2 mW and fixed gate width of 100 ns suggests stronger dressing effect in Pr^{3+}: YPO_4 [13]. Besides, multiple sharp spectral peaks are observed in Pr^{3+}: YPO_4. At gate position of 20 μs, in pure H-phase of Pr^{3+}: YPO_4, spectral filter suggests narrow multi-bandpass notch filter. While, in pure T-phase with increasing gate position

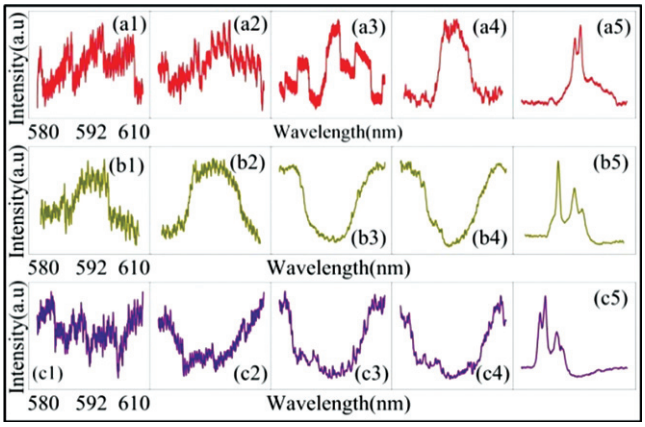

Fig. 7: Spectral intensity signal of the composite signals obtained from Pr^{3+}: YPO_4 measured at different gate positions by fixing the power at 2 mW for (a) H-phase, (b) T-phase, (c) (much H-phase + less T-phase) phase.

from 200 ns (fig. 7(a1)) to 2 μs (fig. 7(a3)), the filter is switched from bandpass to broadband stop filter (broad dip). Further, by increasing the gate position at 20 μs, the filter is switched to narrow multi-bandpass notch filter (two sharp spectral peaks) in fig. 7(a5). When the gate position is fixed at 1 μs (fig. 7(c2)), 2 μs (fig. 7(c3)) and 5 μs (fig. 7(c4)) in mixed phase (much H-phase + less T-phase), the filter works as a broadband stop filter, while increasing the gate position to 20 μs (fig. 7(c5)) the filter is switched to narrow multi-bandpass notch filter (three sharp peaks).

Summary. – In summary, we have demonstrated the spectral nature of composite signals obtained from different phases of Eu^{3+}:YPO_4/Pr^{3+}: YPO_4. Both the crystals were modulated by gate position and gate width. The resolution of the spectral outputs were associated with the number of energy levels and their contribution, controlled through gate width. By changing the gate position, linewidth of the spectral signal, AT splitting, and proportion of Stokes and FL in composite signal were modulated desireably. Further, in the mixed phase of T and H, the H-phase were observed with strong dressing effect suggested by the suppression dips. The tunable spectral filter was realized from the spectral intensity results and controlled by gate position. The bandwidth contrast of the tunable filter is optimized at 93%.

* * *

This work was supported by the National Key R&D Program of China (2017YFA0303700, 2018YFA0307500), National Natural Science Foundation of China (61975159, 61605154, 11604256, 11804267, 11904279).

REFERENCES

[1] Beil Fabian *et al.*, *J. Phys. B*, **41** (2008) 074001.
[2] Sabooni Mahmood *et al.*, *Phys. Rev. Lett.*, **111** (2013) 183602.
[3] Wang Hai-Hua *et al.*, *Appl. Phys. Lett.*, **93** (2008) 221112.
[4] Turukhin A. V. *et al.*, *Phys. Rev. Lett.*, **88** (2001) 023602.
[5] Wang Hai-Hua *et al.*, *Appl. Phys. Lett.*, **92** (2008) 011105.
[6] Ma C.-G. *et al.*, *J. Lumin.*, **152** (2014) 70.
[7] Vanetsev A. S. *et al.*, *J. Alloys Compd.*, **639** (2015) 415.
[8] Yahiaoui Z., Hassairi M. A. and Dammak M., *J. Electron. Mater.*, **46** (2017) 4765.
[9] Arakcheeva Alla *et al.*, *Chem. Sci.*, **3** (2012) 384.
[10] Li Peng *et al.*, *Cryst. Growth Des.*, **17** (2017) 5935.
[11] Yuan Taoli *et al.*, *J. Lumin.*, **201** (2018) 350.
[12] Li Peiying *et al.*, *Opt. Mater.*, **35** (2013) 1062.
[13] Wen Feng *et al.*, *Opt. Lett.*, **40** (2015) 4599.
[14] Moune O. K., Faucher M. D. and Edelstein N., *J. Lumin.*, **96** (2002) 51.
[15] Raza Faizan *et al.*, *Laser Phys. Lett.*, **16** (2019) 055402.
[16] Moune O. K., Faucher M. D. and Edelstein N., *J. Alloys Compd.*, **323** (2001) 783.